VIP Rechargeable Lithium Batteries Very Important Paper

How to cite:
International Edition: doi.org/10.1002/anie.202208743
German Edition: doi.org/10.1002/ange.202208743

The Crucial Role of Electrode Potential of a Working Anode in Dictating the Structural Evolution of Solid Electrolyte Interphase

Shu-Yu Sun, Nao Yao, Cheng-Bin Jin, Jin Xie, Xi-Yao Li, Ming-Yue Zhou, Xiang Chen, Bo-Quan Li, Xue-Qiang Zhang, and Qiang Zhang**

Abstract: The performance of rechargeable lithium (Li) batteries is highly correlated with the structure of solid electrolyte interphase (SEI). The properties of a working anode are vital factors in determining the structure of SEI; however, the correspondingly poor understanding hinders the rational regulation of SEI. Herein, the electrode potential and anode material, two critical properties of an anode, in dictating the structural evolution of SEI were investigated theoretically and experimentally. The anode potential is identified as a crucial role in dictating the SEI structure. The anode potential determines the reduction products in the electrolyte, ultimately giving rise to the mosaic and bilayer SEI structure at high and low potential, respectively. In contrast, the anode material does not cause a significant change in the SEI structure. This work discloses the crucial role of electrode potential in dictating SEI structure and provides rational guidance to regulate SEI structure.

Introduction

With the development of the non-fossil and wireless society, the urgent demand for portable electronics and electric vehicles puts forward a requirement for high-energy-density rechargeable batteries as energy storage devices.[1] However, the energy density of state-of-the-art lithium-ion (Li-ion) batteries based on the chemistry of intercalation anodes gradually approaches the ceiling of 350 $Wh\,kg^{-1}$.[2] Therefore, it is necessary to develop next-generation secondary Li batteries with higher energy density than conventional Li-ion batteries.

An anode with a high specific capacity and an extremely low electrode potential, such as the Li metal anode, is indispensable to further improving the energy density of batteries theoretically.[3] Due to the low electrode potential of the anode, non-aqueous electrolytes can be reduced spontaneously and the decomposition products of electrolytes form a chemically inert layer on the anode, namely the solid electrolyte interphase (SEI).[4] For Li batteries, the physicochemical properties of SEI highly depend on its structure in addition to its components. Meanwhile, the SEI plays a vital role in dictating the performance of anodes and batteries.[5] Concretely, the structure of SEI determines the transport rate and the uniformity of Li ions (Li^+) from the electrolyte to the anode, which significantly affects the rate and polarization of electrochemical reactions at the anode/electrolyte interface.[6] The lifespan of batteries also displays strong dependence on the stability of SEI.[7] Thence, it is important to explore the factors that impact the structure of SEI to further understand the formation mechanism and achieve the rational regulation of SEI.

SEI mainly comprises insoluble decomposition products of electrolyte components, including both Li salts and solvents. In detail, Li salts tend to be reduced into inorganic compounds such as LiF and Li_2O, while solvents can produce both inorganic and organic compounds simultaneously.[8] The inorganic and organic compounds are randomly stacked, forming SEI with different structures. Therefore, electrolyte components are feasible to regulate the structure of SEI. Currently, there are many reports about the influence of electrolytes on the structure of SEI, which is the basis of regulating SEI for stabilizing batteries.[9] For example, a cryo-electron microscope (cryo-EM) revealed that the SEI presented a LiF-rich SEI with bilayer nanostructure due to the addition of fluoroethylene carbonate (FEC).[10] In addition, the application of $LiNO_3$ can also change the structure of SEI into the bilayer model, which was also verified by cryo-EM.[11]

Compared with electrolytes, the evolution of the structure of SEI with the change of anode properties is poorly understood.[12] In a recent review, the similarities and differences of SEI on various metal anodes were summarized. It is believed that the SEI on the surface of multivalent metal anodes (e.g., Mg, Zn, and Al) is more complicated than that on the surface of alkali metal anodes such as Na and K, whose properties are similar to Li.[13] Nonetheless, the

[*] S.-Y. Sun, N. Yao, Dr. C.-B. Jin, J. Xie, X.-Y. Li, Dr. M.-Y. Zhou, Dr. X. Chen, Prof. Q. Zhang
Beijing Key Laboratory of Green Chemical, Reaction Engineering and Technology, Department of Chemical Engineering, Tsinghua University
Beijing 100084 (P. R. China)
E-mail: zhang-qiang@mails.tsinghua.edu.cn
Dr. B.-Q. Li, Dr. X.-Q. Zhang
Advanced Research Institute of Multidisciplinary Science, Beijing Institute of Technology
Beijing 100081 (P. R. China)
E-mail: zhangxq@bit.edu.cn
Dr. B.-Q. Li, Dr. X.-Q. Zhang
School of Materials Science and Engineering, Beijing Institute of Technology
Beijing 100081 (P. R. China)

influence of the properties of a working anode on the structure of SEI is rarely touched. Therefore, investigating the evolution of SEI structure with the change of anode properties will provide a fundamental understanding on the formation mechanism of SEI and rational principles to stabilize SEI.

The electrode potential and anode material are two primary physicochemical properties of a working anode, which directly dictate the structure of SEI. The electrode potential determines the reduction products of electrolytes thermodynamically and affects the structure of SEI.[14] Besides, the anode material may influence the adsorption of electrolyte components on the anode surface, which results in different reduction kinetics of electrolyte components and subsequently the structure of SEI.[15] As a result, the electrode potential and the anode material are selected.

Herein, the role of electrode potential and anode material in dictating the structural evolution of SEI was disclosed. Specifically, graphite and Li are adopted as representative anodes owing to extensive research on them in the field of high-energy-density batteries. Theoretical simulations and experimental investigations confirm that the electrode potential of an anode dominates the structural evolution of SEI. When the electrode potential is changed, the structure of SEI exhibits two different types, the bilayer structure at low potential (<0.1 V vs. Li/Li^+) and the mosaic structure at high potential (3.0 V), respectively. However, the structure evolution of SEI with the change of anode material is little and anode material merely changes the ratio of organic and inorganic compounds in SEI at the same electrode potential of 0 V. These results disclose that the electrode potential of the anode is the crucial factor dictating the structure of SEI.

Results and Discussion

The structure of SEI originates from the stack of both inorganic and organic compounds, which can be vividly described as the "building blocks" of SEI. Recently, Mao and co-workers demonstrated that the content of inorganic and organic compounds in SEI can significantly affect the SEI structure.[16] Therefore, clarifying the influence of an anode on the formation of inorganic and organic compounds in SEI is the precondition to understanding the impact of an anode on the structure of SEI. Note that both inorganic and organic compounds in SEI are from the insoluble reduction products of electrolytes. Owing to the diversity of solvents and Li salts, a representative sample is required to simplify the investigation. Herein, ethylene carbonate (EC) was selected. EC is a well-known carbonate solvent due to its indispensability in forming stable SEI on graphite anodes. In addition, the reduction process of EC has been extensively investigated and the reduction mechanism of EC is relatively more clarified compared with other solvents.[17] When EC undergoes a reduction reaction with the anode, lithium ethylene decarbonate ($(CH_2OCO_2Li)_2$, LEDC) as an organic compound is first formed. Afterward, LEDC can further be reduced to Li_2CO_3.[18] Therefore, LEDC and Li_2CO_3, the direct electrochemical reduction products of EC, are selected to investigate the reduction reaction of EC under different conditions.

To clarify the influence of anode on the formation of inorganic and organic compounds from EC decomposition, the Gibbs free energy change (ΔG) of the reaction producing Li_2CO_3 or LEDC, as a thermodynamic descriptor for evaluating the reaction tendency, is calculated (Figure 1a).[19] The detailed calculation models are listed in the Supporting Information. Here the electrode potential of the Li anode is set to be 0 V, while the electrode potential of lithiated graphite (LiC_6) and delithiated graphite (C_6) was 0.1 and 3.0 V, respectively.[20] All the calculated ΔG are normalized by the number of electrons, and finally obtained the ΔG of the per electron transfer (ΔG_m) of the EC reduction reaction (Figure 1b, Table S1).

To compare the differences in reduction tendency of Li_2CO_3 and LEDC on different anodes, the difference between the ΔG_m of the reduction reaction of EC to Li_2CO_3 and LEDC ($\Delta(\Delta G_m) = \Delta G_m(Li_2CO_3) - \Delta G_m(LEDC)$) on anodes with different properties was further calculated. On Li and LiC_6 with the same electrode potentials, EC shows similar reduction trends. The $\Delta(\Delta G_m)$ of Li and LiC_6 is

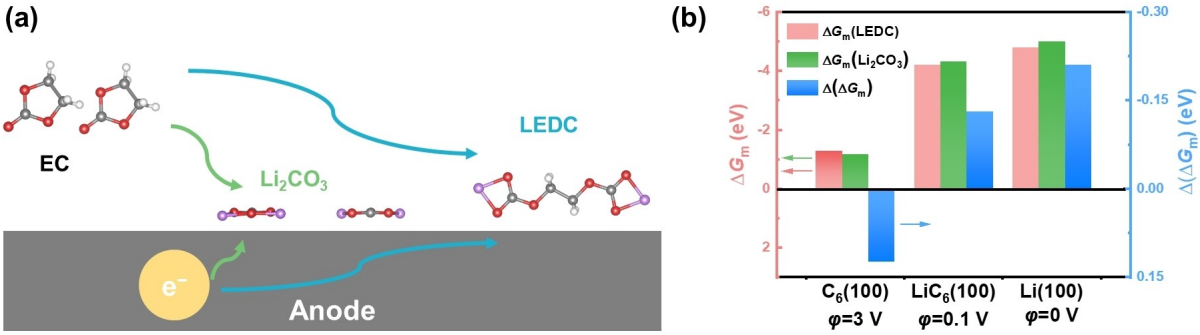

Figure 1. Theoretical calculation of the Gibbs free energy change of the reaction forming LEDC or Li_2CO_3 on different anodes. a) Scheme of the calculation model (red, oxygen; grey, carbon; white, hydrogen; and purple, lithium); b) the free energy calculation results. ΔG_m represents the ΔG of the one-electron reaction in which EC is reduced to the corresponding products. $\Delta(\Delta G_m)$ was calculated by subtracting $\Delta G_m(LEDC)$ from $\Delta G_m(Li_2CO_3)$.

−0.21 eV and −0.13 eV, respectively. Meanwhile, the difference of $\Delta(\Delta G_m)$ between the two anodes is only 0.08 eV, indicating that the reduction trend of EC is not significantly affected by the change of anode material. However, EC shows completely different reduction trends at the same anode with different potentials for the graphite anodes. The $\Delta(\Delta G_m)$ on C_6 is 0.12 eV, which is more positive than that of LiC_6 (−0.13 eV). In addition, the difference of $\Delta(\Delta G_m)$ between LiC_6 and C_6 is up to 0.25 eV, illustrating that EC is more likely to be reduced to inorganic compounds than organic compounds with the change of electrode potential from high to low.

To summarize, the electrode potential of the anode significantly affects the ΔG_m of the reduction reaction of EC on the anode surface, leading to a noticeable change in the building blocks of SEI. Distinctive reduction trends of EC to the inorganic and organic compounds can lead to different ratios of inorganic and organic compounds, which will directly impact the stacking of inorganic and organic compounds on the anode surface, resulting in different structures of SEI.

To investigate the effect of the electrode potentials and material properties of the anode on the SEI structure, respectively, the controlled variable method was used to design the experimental conditions for verifying the calculated results. Firstly, except for electrode potential and anode material, factors interfering with the SEI structure on the anode are excluded. Herein, lithium iron phosphate ($LiFePO_4$, LFP) is employed as the cathode to avoid the disturbance of the dissolved transition metal ions from the cathode in the formation of SEI.[21] Secondly, the components of electrolytes should be simple but representative to form an SEI with a simple structure. As mentioned above, EC is a well-known carbonate solvent with a deep understanding of its decomposition mechanism. However, pure EC is in a solid state at room temperature and thus a co-solvent is necessary for EC-based electrolytes. Moreover, the decomposition products of Li salts should be simple and even negligible. Therefore, 1.0 M $LiPF_6$ in EC/dimethyl carbonate (DEC) with a volume ratio of 1:1 was employed as the electrolyte. In particular, for EC-based electrolytes, the solvation sheath of Li ions mainly consists of EC when the EC content is higher than 30 %, which ensures that the decomposition products of EC dominate the components of SEI because EC can be preferentially reduced compared with DEC as reported.[22] Thirdly, a stable SEI without significant change in components and structure after formation is required. Thus, 5 galvanostatic cycles were conducted at a low current density (0.1 C, Figure S4) to obtain a stable SEI. A low current density can lead to a low overpotential, resulting in the potential of the electrode being closer to its standard electrode potential, which can mitigate the influence of polarization on the formation of SEI. Graphite | LFP cells were assembled to investigate the SEI formed on the graphite anode at different states (Figure S5 and S6). Additionally, the XPS results of the SEI on the graphite anode after 10 cycles are similar to that on the graphite anode after 5 cycles (Figure S7 and S8), which indicates that the SEI obtained after 5 cycles is stable. Finally, multiple parallel experiments were carried out to make the results reproducible (Figure S9).

Graphite anode is chosen owing to its controllable electrode potential to explore the influence of the anode electrode potential on the structure of SEI. The electrode potential of the graphite anode at the charge state of LiC_6 is 0.1 V vs. Li/Li^+, and the electrode potential of the graphite anode at the discharge state of C_6 is 3.0 V vs. Li/Li^+. The components and structure of SEI were detected by in-depth XPS. According to the element distribution at different sputtering times (Figure S5), the element distribution of SEI changes within 40 s of sputtering and maintains stable after 80 s of sputtering.

The distribution of LiF and Li_xPF_y are the same in SEI on LiC_6 and C_6 from the F 1s and P 2p spectra (Figure S6), illustrating that the decomposition products of $LiPF_6$ on two anodes are similar. On the contrary, from the C 1s spectra (Figure S6), the C–O-containing species produced by solvents present different distribution features on two anodes. In the SEI of C_6, the C–O-containing species have relatively high content and are distributed uniformly in space; while in the SEI of LiC_6, the content of C–O-containing species is relatively high on the surface of SEI (next to electrolytes), and there are almost no C–O-containing species in the inner layer of SEI.

The O 1s spectrum can provide information on the content of both organic components (such as C–O-containing species and lithium alkyl carbonates) and inorganic components (such as Li_2O and Li_2CO_3). In addition, the semi-quantitative content of organic and inorganic components in the same spectrum can be acquired. Thus, the O 1s spectra were chosen here for comparing the structure of SEI on LiC_6 and C_6. The SEI of LiC_6 and C_6 exhibit distinct structures from the O 1s spectra (Figure 2a and b). In the SEI of LiC_6, the outer layer contains organic components such as C–O-containing species and LEDC and the inner layer is mainly composed of inorganic components like Li_2O and Li_2CO_3. In comparison, in the SEI of C_6, organic and inorganic species (LEDC and Li_2CO_3) exist at various etching depths. The distribution of organic and inorganic components implies the different structures of SEI in the course of the electrode potential changes, which corresponds to the bilayer structure of SEI on LiC_6 and the mosaic structure of SEI on C_6.

To verify the above speculation about the evolution of the SEI structure of graphite anode, the content of inorganic and organic components in SEI was calculated semi-quantificationally based on XPS results. Due to the hydrolysis of Li_2CO_3, Li_2O is generally detected in SEI, which can be employed to reflect the content of Li_2CO_3.[23] The distribution feature of inorganic components and organic components can be reflected by the distribution of Li_2O and the distribution of C–O-containing species, respectively. In particular, the peaks of Li_2O (528.5 eV) and C–O-containing species (533.5 eV) are far away from the other peaks, which is appropriate for unambiguous peak deconvolution and integration. Based on the atomic ratio of the O element and the peak area ratio of the species in O 1s spectra, the atomic ratio of the corresponding Li_2O and

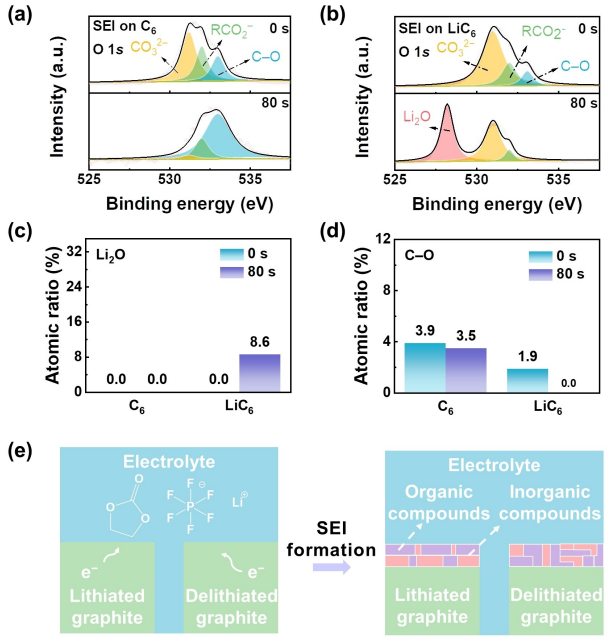

Figure 2. The SEI formed at the different potentials on the graphite anode. The O 1s XPS spectra of SEI on a) C_6 and b) LiC_6 with a sputtering time of 0 and 80 s after 5 cycles. c) The Li_2O and d) C–O-containing species ratio in SEI on C_6 and LiC_6. e) Scheme of the structure of the SEI formed on C_6 and LiC_6.

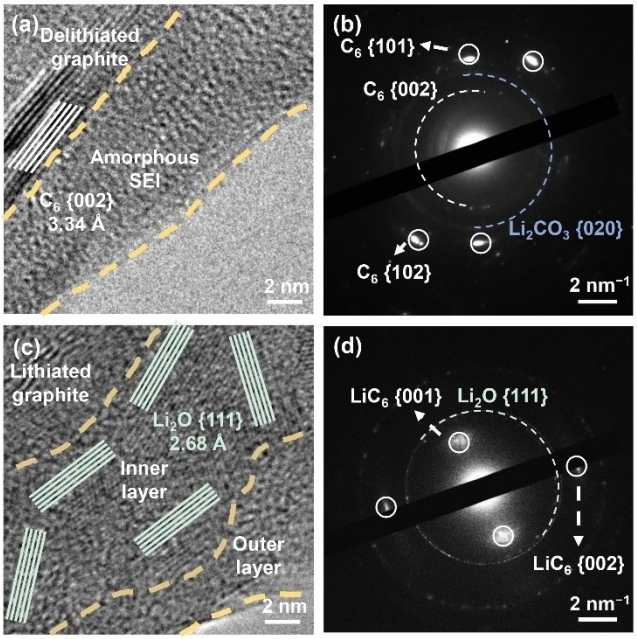

Figure 3. The microstructure of SEI formed at the different potentials on the graphite anode. The cryo-TEM images of SEI on a) C_6 and c) LiC_6 after 5 cycles, which contained crystalline C_6{002}, Li_2O{111} and amorphous region. The SAED image of SEI on b) C_6 and d) LiC_6, in which there are diffraction circles or patterns of Li_2CO_3{020}, C_6{101}, C_6{002}, C_6{102}, LiC_6{001}, LiC_6{002} and Li_2O{111}.

C–O-containing species can be calculated (Table S2). Figure 2c and d represent the atomic ratio of Li_2O and C–O-containing species in SEI on C_6 or LiC_6. For the SEI of LiC_6, the ratio of Li_2O is 8.6 % in the inner layer, which is much higher than that in the outer layer. In contrast, there are many C–O-containing species of 1.9 % in the outer layer whereas no C–O-containing species can be detected in the inner layer, which indicates the bilayer structure of SEI on LiC_6. When it comes to the SEI of C_6, the ratio of C–O species is similar on the surface (3.9 %) and in the inside (3.5 %). Although no Li_2O is observed in both areas, there are other inorganic components like Li_2CO_3. Thus, the components of SEI on C_6 have no obvious differences in the longitudinal distribution, which is different from that on LiC_6. In other words, the structure of SEI on C_6 presents a mosaic structure due to the mixed distribution of organic and inorganic components. Additionally, a similar phenomenon was also observed when the graphite anode was cycled to the 10^{th} cycle (Figure S7 and S8). Therefore, the SEI on LiC_6 presents a bilayer structure with more inorganic compounds in the inner layer and more organic compounds in the outer layer, while the SEI on C_6 exhibits a mosaic structure in which organic and inorganic compounds are mixed. The above results indicate that the evolution of the structure of SEI is notable with the change of electrode potential of the anode.

To observe the microstructure of SEI directly, the SEI on LiC_6 and C_6 was characterized by a cryo-transmission electron microscope (cryo-TEM). Cryo-TEM can provide a nondestructive characterization of the SEI structure.[24] Cryo-TEM images of the SEI (Figure 3a and c) and the corresponding selected area electron diffraction (SAED, Figure 3b, and d) were obtained. The SEI on the surface of C_6 is 10 nm in thickness and there are no significant crystalline species in the SEI according to the cryo-TEM image (Figure 3a). However, the diffraction ring of Li_2CO_3 can be detected (Figure 3b), implying that the SEI contains Li_2CO_3 nanocrystals. Thus, in the SEI of C_6, inorganic compounds are mixed with organic compounds to form an SEI with a mosaic structure. In contrast, the SEI of LiC_6 with a thickness of 15 nm exhibits a completely different structure from the SEI of the C_6. The inner layer is composed of inorganic compounds including crystalline Li_2O (Figure 3c and d) and the outer layer consists of amorphous organic compounds, which together construct an SEI with a bilayer structure.

In summary, the electrode potential of the anode plays an important role in dictating the structure of SEI based on the above results of XPS and cryo-TEM. Therefore, by changing the electrode potential of the anode, the SEI structure undergoes obvious evolution. When the electrode potential of the anode is as low as 0.1 V vs. Li/Li^+, the SEI trends to become a bilayer structure; a mosaic structure forms when the electrode potential of the anode is as high as 3.0 V vs. Li/Li^+ (Figure 2e).

To investigate the evolution of the structure of SEI with the change of anode material, Li anode and graphite anode were selected. The Li anode maintained the potential of about 0 V vs. Li/Li^+ during cycling. Thus, it is necessary to control the potential of graphite anode (C_6) to be consistent with that of Li anode to explore the effect of anode material

on the structure of SEI. Consequently, the C_6 | Li cells were assembled, in which the graphite electrode was used as the working electrode and the lithium metal electrode was used as the counter electrode. Then, a constant voltage of 0 V was applied to force the graphite anode to remain at the same potential as the lithium metal electrode, excluding the influence of different electrode potentials during the formation of SEI (Figure S11). To ensure that there is no Li deposition during the constant-voltage of the 0 V process which will influence the formation of SEI, the scanning electron microscope (SEM) and X-ray diffraction spectrum (XRD) were used to analyze the composition of graphite anode after the constant-voltage process. According to the results from SEM (Figure S12) and XRD (Figure S13), there was no Li deposition, which indicates that the formation of SEI during this process solely happened on the graphite anode but not on the deposited Li. For the Li anode, the SEI was obtained from Li | LFP full-cells at the same test conditions as graphite | LFP full-cells (Figure S14). Parallel experiments verify the reproducibility of the SEI of Li (Figure S15). The structure of SEI on Li in the discharged state was also characterized (Figure S16). The XPS results confirm that the SEI of Li in the discharge state is similar to that in the charge state, indicating that it is reasonable to analyze the SEI of Li in the charge state. Therefore, the SEI of the graphite anode constructed by the constant voltage method (marked as LiC_6 at 0 V) and the SEI of the Li anode are compared in detail.

As mentioned before, the distribution of reduction products of Li salts is also similar in SEI on LiC_6 at 0 V and Li from the F 1s spectra and P 2p spectra (Figure S18). But interestingly, the C 1s and O 1s spectra of the SEI of the two anodes are also quite similar (Figure S18). From the C 1s spectra, the SEI of LiC_6 at 0 V and the SEI of Li both exhibit a high content of C–O-containing species in the outer layer, while almost no signal of C–O-containing species can be detected in the inner layer. Using the same method as previously, the composition and structure of the SEI of the two anodes are quantitatively analyzed by O 1s spectra.

The difference in SEI between the two anodes is further analyzed by O 1s spectra. Figure 4a and b present the O 1s spectra of SEI on Li and LiC_6 at 0 V. The SEI on Li and LiC_6 at 0 V exhibit a similar distribution of compounds, which is also investigated in C 1s spectra (Figure S18). The outer layer of SEI is composed of organic compounds such as C–O-containing species and alkyl lithium carbonate ($ROCO_2Li$), while the inner layer is mainly composed of inorganic compounds containing Li_2O and Li_2CO_3. Figure 4c and d exhibit the content of inorganic and organic compounds in the inner layer and outer layer of the SEI on the two anodes. Both SEI of LiC_6 at 0 V and Li present a bilayer structure with more organic compounds in the outer layer (4.4 % for SEI of Li and 4.6 % for SEI of LiC_6 at 0 V) and more inorganic compounds in the inner layer (16.8 % for SEI of Li and 7.0 % for SEI of LiC_6 at 0 V), which is similar to the SEI of LiC_6. It is inferred that when the electrode potential of the anode is closed, the SEI will present a similar structure. By further comparing the composition of

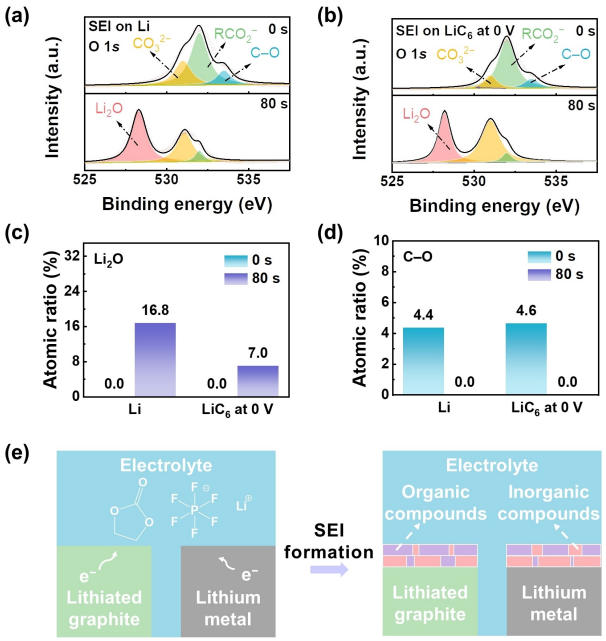

Figure 4. The SEI formed on different anodes at the same potential (0 V vs. Li^+/Li). The O 1s XPS spectra of SEI on a) Li and b) LiC_6 at 0 V. c) The Li_2O and d) C–O-containing species ratio in SEI. e) Scheme of the structure of the SEI formed on Li and LiC_6 at 0 V.

the SEI of the two anodes, it can be observed that the content of inorganic compounds of the SEI on Li is about 2 times higher than that of the SEI on LiC_6 at 0 V in the inner layer. However, the content of organic compounds of SEI on two anodes is similar in the outer layer. These results directly illustrate that the ratio of inorganic and organic components in the SEI of Li is higher than that in the SEI of LiC_6 at 0 V. Therefore, it can be inferred that the change of anode material does not cause the obvious evolution of SEI structure, but it can change the ratio of inorganic and organic compounds in the SEI.

To further investigate the microstructure of the SEI, the cryo-TEM images of the SEI (Figure 5a and c) and the corresponding image of SAED (Figure 5b and d) were obtained by cryo-TEM. For the SEI of Li, a layer with about 30 nm in thickness can be observed on the surface of crystalline Li, which is consisted of two layers, i.e., an inner layer, which is mainly consisted of crystalline Li_2O, and an outer layer, which is composed of amorphous organic compounds (Figure 5a and b). Similarly, for the SEI of LiC_6 at 0 V, an SEI with about 10 nm in thickness is also observed, of which the inner layer was composed of crystalline Li_2O and the outer layer was composed of amorphous organic compounds (Figure 5c and d). The cryo-TEM results indicate that the SEI in both Li and LiC_6 at 0 V has a similar bilayer structure, with the outer layer of amorphous organic compounds and the inner layer of inorganic compounds.

The evolution of the structure of SEI with the change of anode material is investigated by XPS and cryo-TEM (Figure 4e). There is little structural evolution of SEI with the change of anode material, which is evidenced by the SEI

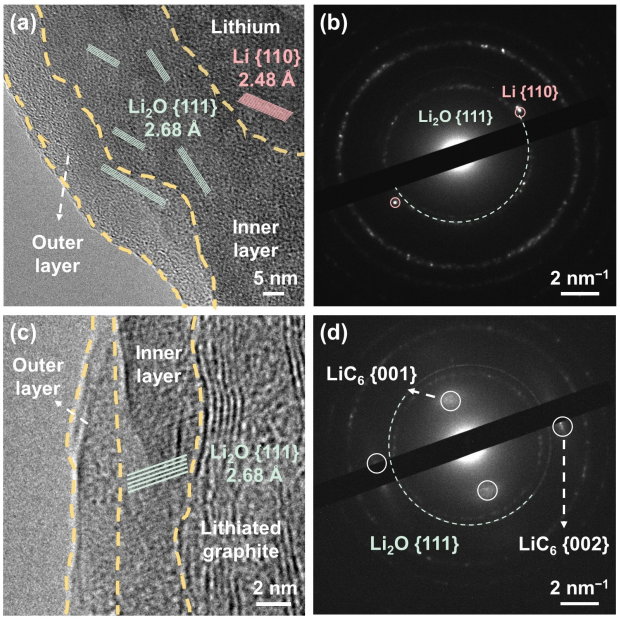

Figure 5. Microstructure of SEI formed on different anodes at the same potential (0 V vs. Li^+/Li). The cryo-TEM of SEI on a) Li and c) LiC_6 at 0 V, which both contained crystalline $Li_2O\{111\}$ and an amorphous region. The SAED image of SEI on b) Li and d) LiC_6 at 0 V, in which there are diffraction circles or patterns of $Li\{110\}$, $Li_2O\{111\}$, $LiC_6\{001\}$ and $LiC_6\{002\}$.

with a quite similar bilayer structure on both Li and LiC_6 at 0 V. However, the anode material affects the ratio of inorganic compounds and organic compounds in the SEI. The content of inorganic compounds is about 2 times higher in the inner layer of SEI of Li than that of LiC_6 at 0 V, while the content of organic compounds in the outer layer is similar.

The evolution of the SEI structure with the change of electrode potential and anode materials is summarized (Figure 6). With the change in the electrode potential of the anode, the evolution of the structure of SEI is particularly obvious. When the potential is very low (<0.1 V vs. Li/Li^+), both the lithium metal anode and the graphite anode present the SEI with a bilayer structure. The organic and inorganic compounds are abundant in the outer and inner layer of SEI, respectively. When the potential is high (3.0 V vs. Li/Li^+), the SEI on the graphite anode exhibits a mosaic structure of mixed inorganic and organic compounds. Therefore, the structure of SEI is mainly dominated by the electrode potential of the anode because the electrode potential influences the electrochemical potential of the electron and then changes the ΔG_m of the reduction reaction of the electrolyte component. When the electrode potential is low enough (about 0 V vs. Li/Li^+), the ΔG_m of the reduction reactions to generate inorganic components is more negative than that of organic components, which indicates that the inorganic components are inclined to be primarily generated on the surface of the anode. Consequently, the SEI finally evolves into the bilayer structure. In contrast, when the electrode potential is high (for example 3 V vs. Li/Li^+), electrolyte components can produce organic and inorganic compounds simultaneously, leading to the mixed blocking of organic and inorganic compounds, which causes the SEI change into the mosaic structure. Additionally, there is little structural evolution of SEI with the change of anode material although it can impact the ratio of inorganic and organic components in SEI. Therefore, the structure of SEI is mainly controlled by the electrode potential of the anode. This conclusion is speculated to be generalized to other anode systems, such as silicon anodes. The ΔG of the reduction reaction of electrolyte is directly affected by the electrochemical potential of the electrons in anode. Meanwhile, the electrochemical potential of the electrons is mainly determined by the potential of the anode. However, when the potential is the same, the change of the anode material has little effect on the electrochemical potential of the electrons. Therefore, the electrode potential is the main factor dictating the SEI structure.

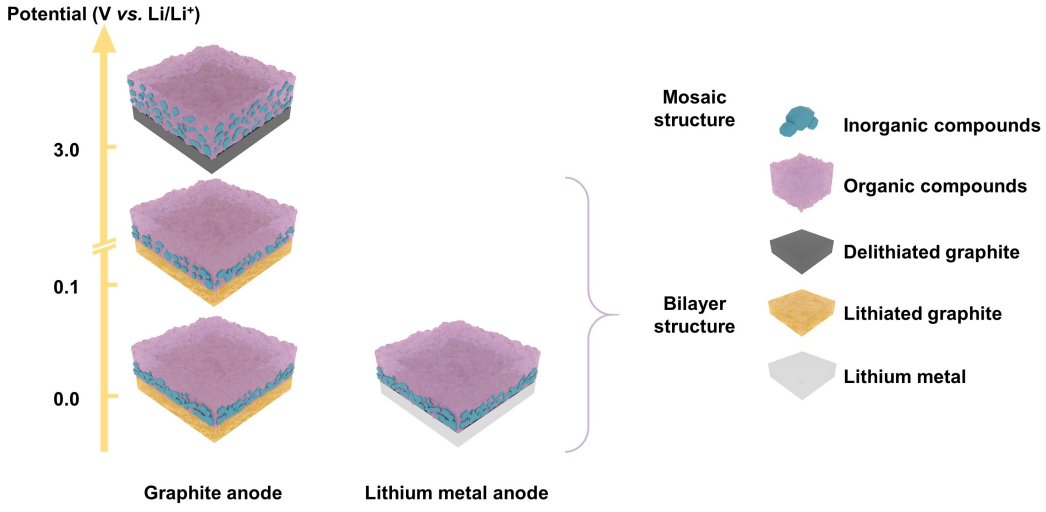

Figure 6. Scheme of the evolution of SEI structure with the change of electrode potential and anode materials.

Unveiling the evolution of the SEI structure with the change of properties of the anode illustrates the key factor of the anode in dictating the SEI structure, which provides fresh insight into the failure mechanism of the anode and guidance to manipulate the structure of the SEI. For example, the potential of anode significantly increases and deviates from the equilibrium potential after long cycles due to the continuous side reactions in batteries. After long cycles, the potential of anodes will be more negative during the charging process. The change of the potential of the anode may lead to the transformation of the SEI structure, thus changing the resistance and uniformity of Li ions in SEI and deteriorating the stability of the anode. Furthermore, this work will provide solid support for manipulating the structure of SEI by rationally controlling the electrode potential of the anode. SEI with different structures can be obtained to adapt different battery systems. For example, LiF is considered to be an effective component in SEI to stabilize lithium metal anodes.[25] A single-layer LiF-dominated SEI can be prepared by controlling the electrode potential to make fluorine-rich Li salts (such as $LiPF_6$) to generate LiF at a set potential because Li salts are generally reduced preferentially compared with solvents.

Conclusion

In conclusion, the role of electrode potential and anode material in dictating the structural evolution of SEI was disclosed by theoretical calculations and experiments. The electrode potential of the anode will significantly affect the ΔG_m of the reduction reaction of solvents on the anode surface, resulting in a significant change in the building blocks of SEI. In addition, by combining the control variable method and the characterization of SEI by XPS and cryo-TEM, it is found that the electrode potential of anodes dominates the evolution of SEI structure. When the electrode potential is low (<0.1 V vs. Li/Li^+), the SEI presents a bilayer structure. However, when the electrode potential is high (3.0 V vs. Li/Li^+), the SEI presents a mosaic structure. In contrast, the anode material merely changes the ratio of organic and inorganic compounds in SEI. This work discloses the evolution of the SEI structure with the change of anode properties, indicates that the electrode potential of a working anode dominates the SEI structure, and provides rational guidance to regulate the structure of SEI.

Acknowledgements

This work was supported by National Key Research and Development Program (2021YFB2500300 and 2021YFB2400300), National Natural Science Foundation of China (52103342, 22109007, and U1801257), China Postdoctoral Science Foundation (BX2021136, 2021M700404, and 2021M691712), and Beijing Municipal Natural Science Foundation (Z200011). The authors acknowledged the support from Tsinghua National Laboratory for Information Science and Technology for theoretical simulations and Beijing Institute of Technology Research Fund Program for Young Scholars. The authors also acknowledge the support of the in situ device XPS from the Analysis Center of Tsinghua University.

Conflict of Interest

The authors declare no conflict of interest.

Data Availability Statement

The data that support the findings of this study are available from the corresponding author upon reasonable request.

Keywords: Anode/Electrolyte Interface · Electrode Potential · Lithium Batteries · Solid Electrolyte Interphase · Structure Evolution

[1] a) J. M. Tarascon, M. Armand, *Nature* **2001**, *414*, 359–367; b) M. Li, J. Lu, Z. Chen, K. Amine, *Adv. Mater.* **2018**, *30*, 1800561; c) S. Chu, A. Majumdar, *Nature* **2012**, *488*, 294–303; d) M. S. Whittingham, *Chem. Rev.* **2004**, *104*, 4271–4302; e) B. Scrosati, J. Hassoun, Y.-K. Sun, *Energy Environ. Sci.* **2011**, *4*, 3287–3295.

[2] a) M. Winter, B. Barnett, K. Xu, *Chem. Rev.* **2018**, *118*, 11433–11456; b) Y. Guo, H. Li, T. Zhai, *Adv. Mater.* **2017**, *29*, 1700007; c) J. Liu, Z. Bao, Y. Cui, E. J. Dufek, J. B. Goodenough, P. Khalifah, Q. Li, B. Y. Liaw, P. Liu, A. Manthiram, Y. S. Meng, V. R. Subramanian, M. F. Toney, V. V. Viswanathan, M. S. Whittingham, J. Xiao, W. Xu, J. Yang, X.-Q. Yang, J.-G. Zhang, *Nat. Energy* **2019**, *4*, 180–186; d) S. J. An, J. Li, C. Daniel, D. Mohanty, S. Nagpure, D. L. Wood, *Carbon* **2016**, *105*, 52–76.

[3] a) J. B. Goodenough, Y. Kim, *Chem. Mater.* **2010**, *22*, 587–603; b) Z. Wang, Z. Sun, J. Li, Y. Shi, C. Sun, B. An, H.-M. Cheng, F. Li, *Chem. Soc. Rev.* **2021**, *50*, 3178–3210; c) J. Popovic, *Nat. Commun.* **2021**, *12*, 6240; d) D. Yuan, Y. Dou, Z. Wu, Y. Tian, K.-H. Ye, Z. Lin, S. X. Dou, S. Zhang, *Chem. Rev.* **2022**, *122*, 957–999; e) X.-Y. Li, S. Feng, M. Zhao, C.-X. Zhao, X. Chen, B.-Q. Li, J.-Q. Huang, Q. Zhang, *Angew. Chem. Int. Ed.* **2022**, *61*, e202114671; *Angew. Chem.* **2022**, *134*, e202114671.

[4] a) X.-B. Cheng, R. Zhang, C.-Z. Zhao, Q. Zhang, *Chem. Rev.* **2017**, *117*, 10403–10473; b) E. Peled, S. Menkin, *J. Electrochem. Soc.* **2017**, *164*, A1703–A1719; c) X. He, D. Bresser, S. Passerini, F. Baakes, U. Krewer, J. Lopez, C. T. Mallia, Y. Shao-Horn, I. Cekic-Laskovic, S. Wiemers-Meyer, F. A. Soto, V. Ponce, J. M. Seminario, P. B. Balbuena, H. Jia, W. Xu, Y. Xu, C. Wang, B. Horstmann, R. Amine, C.-C. Su, J. Shi, K. Amine, M. Winter, A. Latz, R. Kostecki, *Nat. Rev. Mater.* **2021**, *6*, 1036–1052.

[5] a) M. D. Tikekar, S. Choudhury, Z. Tu, L. A. Archer, *Nat. Energy* **2016**, *1*, 16114; b) Y.-X. Yao, C. Yan, Q. Zhang, *Chem. Commun.* **2020**, *56*, 14570–14584; c) M. Gauthier, T. J. Carney, A. Grimaud, L. Giordano, N. Pour, H.-H. Chang, D. P. Fenning, S. F. Lux, O. Paschos, C. Bauer, F. Maglia, S. Lupart, P. Lamp, Y. Shao-Horn, *J. Phys. Chem. Lett.* **2015**, *6*, 4653–4672.

[6] a) H. Bryngelsson, M. Stjerndahl, T. Gustafsson, K. Edström, *J. Power Sources* **2007**, *174*, 970–975; b) Z. Li, J. Huang, B. Yann Liaw, V. Metzler, J. Zhang, *J. Power Sources* **2014**, *254*,

168–182; c) G. Yasin, M. Arif, T. Mehtab, X. Lu, D. Yu, N. Muhammad, M. T. Nazir, H. Song, *Energy Storage Mater.* **2020**, *25*, 644–678.
[7] a) W. Liu, P. Liu, D. Mitlin, *Adv. Energy Mater.* **2020**, *10*, 2002297; b) P. Verma, P. Maire, P. Novák, *Electrochim. Acta* **2010**, *55*, 6332–6341; c) T. Li, X.-Q. Zhang, P. Shi, Q. Zhang, *Joule* **2019**, *3*, 2647–2661.
[8] a) K. Xu, *Chem. Rev.* **2014**, *114*, 11503–11618; b) X.-B. Cheng, R. Zhang, C.-Z. Zhao, F. Wei, J.-G. Zhang, Q. Zhang, *Adv. Sci.* **2016**, *3*, 1500213; c) S. K. Heiskanen, J. Kim, B. L. Lucht, *Joule* **2019**, *3*, 2322–2333.
[9] a) X.-Q. Zhang, X.-B. Cheng, Q. Zhang, *Adv. Mater. Interfaces* **2018**, *5*, 1701097; b) M. S. Kim, Z. Zhang, P. E. Rudnicki, Z. Yu, J. Wang, H. Wang, S. T. Oyakhire, Y. Chen, S. C. Kim, W. Zhang, D. T. Boyle, X. Kong, R. Xu, Z. Huang, W. Huang, S. F. Bent, L.-W. Wang, J. Qin, Z. Bao, Y. Cui, *Nat. Mater.* **2022**, *21*, 445–454; c) S. Tan, Z. Shadike, J. Li, X. Wang, Y. Yang, R. Lin, A. Cresce, J. Hu, A. Hunt, I. Waluyo, L. Ma, F. Monaco, P. Cloetens, J. Xiao, Y. Liu, X.-Q. Yang, K. Xu, E. Hu, *Nat. Energy* **2022**, *7*, 484–494; d) T. Zhou, Y. Zhao, M. El Kazzi, J. W. Choi, A. Coskun, *Angew. Chem. Int. Ed.* **2022**, *61*, e202115884; *Angew. Chem.* **2022**, *134*, e202115884.
[10] Y. Li, W. Huang, Y. Li, A. Pei, D. T. Boyle, Y. Cui, *Joule* **2018**, *2*, 2167–2177.
[11] Y. Liu, D. Lin, Y. Li, G. Chen, A. Pei, O. Nix, Y. Li, Y. Cui, *Nat. Commun.* **2018**, *9*, 3656.
[12] P. Zhai, L. Liu, X. Gu, T. Wang, Y. Gong, *Adv. Energy Mater.* **2020**, *10*, 2001257.
[13] Q. Zhao, S. Stalin, L. A. Archer, *Joule* **2021**, *5*, 1119–1142.
[14] a) T. Liu, L. Lin, X. Bi, L. Tian, K. Yang, J. Liu, M. Li, Z. Chen, J. Lu, K. Amine, K. Xu, F. Pan, *Nat. Nanotechnol.* **2019**, *14*, 50–56; b) A. V. Cresce, S. M. Russell, D. R. Baker, K. J. Gaskell, K. Xu, *Nano Lett.* **2014**, *14*, 1405–1412.
[15] T. Placke, V. Siozios, R. Schmitz, S. F. Lux, P. Bieker, C. Colle, H. W. Meyer, S. Passerini, M. Winter, *J. Power Sources* **2012**, *200*, 83–91.
[16] W.-W. Wang, Y. Gu, J.-H. Wang, Z.-B. Chen, X.-T. Yin, Q.-H. Wu, J.-W. Yan, B.-W. Mao, *J. Electrochem. Soc.* **2022**, *169*, 020563.
[17] Y. Surace, D. Leanza, M. Mirolo, Ł. Kondracki, C. A. F. Vaz, M. El Kazzi, P. Novák, S. Trabesinger, *Energy Storage Mater.* **2022**, *44*, 156–167.
[18] a) G. V. Zhuang, K. Xu, H. Yang, T. R. Jow, P. N. Ross, *J. Phys. Chem. B* **2005**, *109*, 17567–17573; b) K. Leung, *J. Phys. Chem. C* **2013**, *117*, 1539–1547; c) S. S. Zhang, *J. Power Sources* **2006**, *162*, 1379–1394.
[19] a) T. Li, P. B. Balbuena, *Chem. Phys. Lett.* **2000**, *317*, 421–429; b) Y. Wang, S. Nakamura, M. Ue, P. B. Balbuena, *J. Am. Chem. Soc.* **2001**, *123*, 11708–11718.
[20] S. Zhang, M. S. Ding, K. Xu, J. Allen, T. R. Jow, *Electrochem. Solid-State Lett.* **2001**, *4*, A206–A208.
[21] X.-Q. Zhang, X.-M. Wang, B.-Q. Li, P. Shi, J.-Q. Huang, A.-B. Chen, Q. Zhang, *J. Mater. Chem. A* **2020**, *8*, 4283–4289.
[22] a) J. Ming, Z. Cao, Q. Li, W. Wahyudi, W. Wang, L. Cavallo, K.-J. Park, Y.-K. Sun, H. N. Alshareef, *ACS Energy Lett.* **2019**, *4*, 1584–1593; b) K. Xu, *J. Electrochem. Soc.* **2007**, *154*, A162–A167.
[23] a) D. M. Seo, D. Chalasani, B. S. Parimalam, R. Kadam, M. Nie, B. L. Lucht, *ECS Electrochem. Lett.* **2014**, *3*, A91–A93; b) K. Xu, G. V. Zhuang, J. L. Allen, U. Lee, S. S. Zhang, P. N. Ross, T. R. Jow, *J. Phys. Chem. B* **2006**, *110*, 7708–7719.
[24] a) X.-C. Ren, X.-Q. Zhang, R. Xu, J.-Q. Huang, Q. Zhang, *Adv. Mater.* **2020**, *32*, 1908293; b) M. J. Zachman, Z. Tu, S. Choudhury, L. A. Archer, L. F. Kourkoutis, *Nature* **2018**, *560*, 345–349.
[25] a) Z. Yu, P. E. Rudnicki, Z. Zhang, Z. Huang, H. Celik, S. T. Oyakhire, Y. Chen, X. Kong, S. C. Kim, X. Xiao, H. Wang, Y. Zheng, G. A. Kamat, M. S. Kim, S. F. Bent, J. Qin, Y. Cui, Z. Bao, *Nat. Energy* **2022**, *7*, 94–106; b) X.-Q. Zhang, X.-B. Cheng, X. Chen, C. Yan, Q. Zhang, *Adv. Funct. Mater.* **2017**, *27*, 1605989.

Manuscript received: June 14, 2022
Accepted manuscript online: August 12, 2022
Version of record online: ■■, ■■

Research Articles

Rechargeable Lithium Batteries

S.-Y. Sun, N. Yao, C.-B. Jin, J. Xie, X.-Y. Li, M.-Y. Zhou, X. Chen, B.-Q. Li, X.-Q. Zhang,* Q. Zhang* e202208743

The Crucial Role of Electrode Potential of a Working Anode in Dictating the Structural Evolution of Solid Electrolyte Interphase

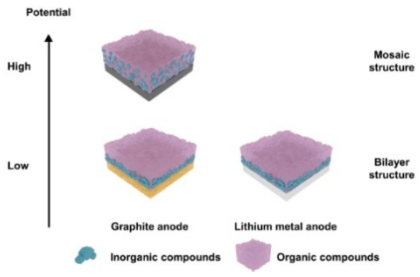

The role of electrode potential and anode material, two critical properties of a working anode, in dictating the structural evolution of solid electrolyte interphase (SEI) was investigated theoretically and experimentally, which provides rational guidance to regulate SEI structure.